Additive Manufacturing: Metallurgy, Cut Analysis & Porosity

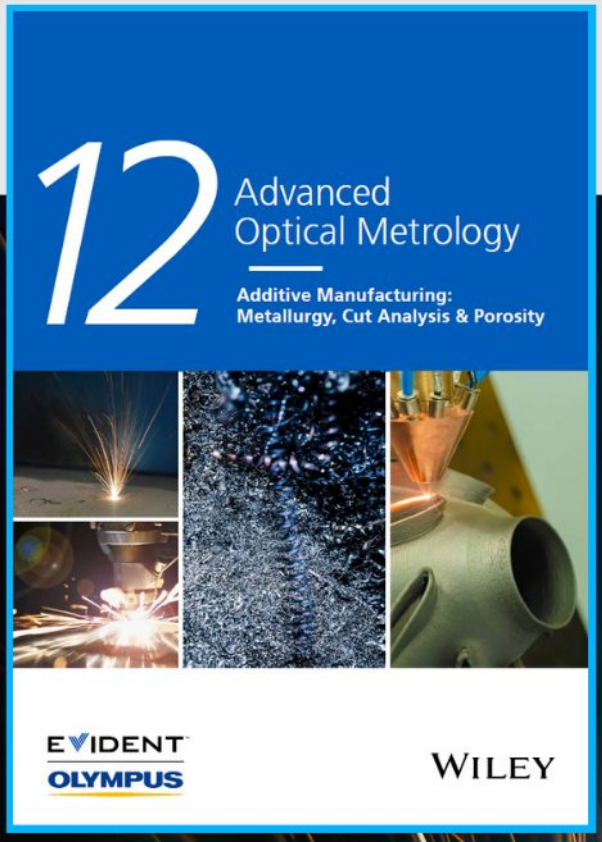

The latest eBook from Advanced Optical Metrology. Download for free.

In industry, sector after sector is moving away from conventional production methods to additive manufacturing, a technology that has been recommended for substantial research investment.

Download the latest eBook to read about the applications, trends, opportunities, and challenges around this process, and how it has been adapted to different industrial sectors.

EVIDENT
OLYMPUS

WILEY

ADVANCED FUNCTIONAL MATERIALS
www.afm-journal.de

Semi-Crystalline Rubber as a Light-Responsive, Programmable, Resilient Robotic Material

Qi Yang, Hamed Shahsavan, Zixuan Deng, Hongshuang Guo, Hang Zhang, Heng Liu, Chunyu Zhang, Arri Priimagi, Xuequan Zhang, and Hao Zeng**

Polymers with large and reversible light-induced deformation offer a plethora of opportunities for the wireless control of small-scale soft robots. However, their widespread adoption in real-world applications is hindered, mainly due to their intrinsic softening upon illumination. Such limitation has detrimental effects on the achievable stress, durability, and precise positional control of the soft actuators after multiple cycles of use. Here, a synthetic rubber from a polybutadiene-polyethylene copolymer is reported as a durable material for light-controlled soft robots. The rubber can be programmed to exhibit various deformation modes controlled by visible-to-infrared light through a photothermal effect. Semi-crystallinity of polyethylene within the rubbery network provides this material with a remarkable modulus at high temperatures (2.5 MPa at 100–140 °C), deformation repeatability (>90%) and shape-recovery (>98%) after 100 actuation cycles subject to loads ranging from 10 to 10 000 times of its body weight (1.4 kPa–1.4 MPa). Soft robotic applications are demonstrated, such as thermally-driven jumping and photo-driven cargo transport carrying up to 1200 times its own weight. The results expand the portfolio of materials in designing remotely-controlled, robust, and resilient soft robots working at small scales.

1. Introduction

The emergence of small-scale soft robots has brought about a wealth of possibilities for safe interaction between robots and humans.[1–3] Owing to their softness and size, such robots can perform a range of delicate tasks in tiny and constrained environments. In long term, they are expected to revolutionize healthcare by offering targeted and minimally invasive procedures.[4] Despite great progress in developing various powering, monitoring, and manipulation techniques, the synthesis of novel robotic materials is one of the most pressing issues in small-scale soft robotics.[5] Such materials are typically made of stimuli-responsive polymers with embedded sensing and actuation capabilities.[6] Their actuation performance can be precisely programmed, and they can be miniaturized via different microfabrication techniques.[7–9] Accordingly, such polymers are important candidates for realizing wirelessly controlled soft actuators with much smaller sizes than their pneumatic and dielectric counterparts.[2,4]

The actuation mechanism in the majority of stimuli-responsive polymers is rooted in reversible phase transitions, such as glass transition in shape memory polymers (SMPs),[10,11] nematic-to-isotropic transition in liquid crystal elastomers (LCEs),[12,13] and coil-to-globule transition in hydrogels.[14,15] Such phase transitions are typically triggered by heat and manifest themselves in reversible strain or shape changes. Nowadays, LCEs are commonly used responsive materials in soft small-scale robotics, thanks to their large, reversible, and programmable deformation in response to various stimuli such as heat, light, and electric fields.[16–20] Such properties are rooted in the anisotropic ordering of their molecules locked in an elastic network. Disruptions in the molecular alignment result in various modes of deformation such as expansion/contraction, bending, and twisting.[21,22] These deformation profiles have been deployed for a variety of soft robotic locomotion modes, such as walking, swimming, and jumping, in addition to functions such as gripping and cargo transport.[23–29]

Despite such achievements, stimuli-responsive polymers still face challenges in their widespread adoption of real-world soft robotic applications. Softening and dramatic decrease in the modulus (E) of such polymers upon heating

Q. Yang, H. Liu, C. Zhang, X. Zhang
Key Lab of Rubber-Plastics, Ministry of Education/Shandong Provincial Key Lab of Rubber-plastics, School of Polymer Science and Engineering
Qingdao University of Science & Technology
Qingdao 266042, China
E-mail: hengliu@qust.edu.cn
H. Shahsavan
Department of Chemical Engineering & Waterloo Institute for Nanotechnology
University of Waterloo
Waterloo, ON N2L 3G1, Canada
Z. Deng, H. Guo, A. Priimagi, H. Zeng
Smart Photonic Materials
Faculty of Engineering and Natural Sciences
Tampere University
Tampere P.O. Box 541, FI-33101, Finland
E-mail: hao.zeng@tuni.fi
H. Zhang
Department of Applied Physics
Aalto University
P.O. Box 15100, Espoo FI 02150, Finland
The ORCID identification number(s) for the author(s) of this article can be found under https://doi.org/10.1002/adfm.202206939.

© 2022 The Authors. Advanced Functional Materials published by Wiley-VCH GmbH. This is an open access article under the terms of the Creative Commons Attribution License, which permits use, distribution and reproduction in any medium, provided the original work is properly cited.

DOI: 10.1002/adfm.202206939

Check for updates
16163028, 2022, 41, Downloaded from https://onlinelibrary.wiley.com/doi/10.1002/adfm.202206939 by Tampere University Of Tech Tut, Wiley Online Library on [25/10/2022]. See the Terms and Conditions (https://onlinelibrary.wiley.com/terms-and-conditions) on Wiley Online Library for rules of use; OA articles are governed by the applicable Creative Commons License

16163028, 2022, 41, Downloaded from https://onlinelibrary.wiley.com/doi/10.1002/adfm.202206939 by Tampere University Of Tech Tut, Wiley Online Library on [25/10/2022]. See the Terms and Conditions (https://onlinelibrary.wiley.com/terms-and-conditions) on Wiley Online Library for rules of use; OA articles are governed by the applicable Creative Commons License

or illumination[30–32] is one of the major drawbacks that diminishes their performance. For instance, the output work of LCEs, W_{out} (proportional to E) could considerably decrease when they soften at elevated temperatures.[33] Soft actuators essentially function through active strains, during which they are constantly subject to external forces such as friction, adhesion, or load-bearing during motion. Thermal softening not only curtails actuator' ability to withstand such external forces, but also adversely affects their durability, actuation repeatability, and shape-recovery over multiple cycles of use, or active strain. As such, a solution to remedy all these issues is highly desired.

Herein, we report a synthetic rubber from poly(ethylene-co-butadiene) (PEB), which has similar characteristics to LCEs (anisotropy, programmed and reversible deformation, and large shape-change) and exhibits remarkable durability and resilience. This material consists of rubbery domains of polybutadiene and semi-crystalline domains of polyethylene, cross-linked by a photothermal croconaine dye. The pre-strain in the rubbery domains along with the melting/crystallization of the semi-crystalline domains enable reversible deformations with various programmable modes, in response to photothermal heating. The material possesses high modulus and strains even at elevated temperatures (2.5 MPa and 28% at 140 °C), excellent actuation repeatability (>90%), and shape-recovery (>98%) over 100 actuation cycles subject to loads ranging over four orders of magnitude (1.4 kPa–1.4 MPa). As a proof-of-concept, we deployed these rubbers in soft robotic applications such as locomotion by crawling or jumping and cargo transport by carrying loads up to 1200 times their own weight. Our results offer a new robust material for small-scale soft robots that can be manipulated wirelessly by stimuli such as light.

2. Results

2.1. Synthesis of the Responsive Rubber

Synthetic rubbers are artificial elastomers, produced by polymerization of petroleum-based monomers.[34] Similar to natural rubbers, they possess stable physical and chemical properties and high mechanical resilience.[35] Synthetic rubbers are also superior to their natural counterparts in resistance to wear and ozone cracking. They are also amenable to the engineering of their functional constituents,[36] which facilitates their application in various user products such as roof covers, tires, and shoes.[37] Plastics are polymeric materials with different mechanical properties below and above their glass transition temperature.[38] Polyethylene (PE) is a common semi-crystalline plastic with relatively low material hardness and resilience most often used in our daily life. The mechanical stability of PE can be tuned by the molecular weight or branching degree, which affects its melting point (typically in the range of 100 to 130 °C).[39] Many cross-linked networks of semi-crystalline polymers benefit from stable physicochemical properties,[40] and synthetic rubbers from thermally triggered deformation and resilience.[41]

Cross-linking of copolymers made from rubbery segments (polybutadiene, PB, in our case), and semi-crystalline segments (PE), yields networks capable of two-way shape memory and reversible (photo-)thermoresponsive deformations.[42,43] A sketch of such a cross-linked network is illustrated in **Figure 1**a, where crystalline domains formed by the PE segments gradually melt upon heating and drive the system toward disorder. Due to the entropic elasticity, the cross-linked chains in the rubber contract along the pre-stretched direction upon heating and expand in the perpendicular direction (Figure 1b). In this system, chemical cross-linking increases the toughness and allows for reversible shape-change to be obtained. Upon cooling, the PE segments re-crystallize, the rubbery chains return to the original state fixed by the cross-links and the sample retains the original dimensions.

Figure 1c presents the scheme for the synthesis of photo-responsive poly(ethylene-co-butadiene) rubbers (PEB). In the first step, we used the hydrogenation reaction of cis-1,4-polybutadiene (CPB) chains to create cis-1,4-polyethylene-polybutadiene (PEB) with randomly distributed chain blocks of polyethylene. In the next step, we used a photothermal croconaine dye,[44] 2,5-Bis[(6-thiolhexyl-4-carboxylate-piperidylamino) thiophenyl]-croconium (TTC), to chemically cross-link the network via UV-assisted thiol-ene reaction, to obtain PEB-TTC. The cross-linking process was carried out under three different pre-straining conditions (0%, 50%, and 100%). The details of the synthesis protocol and the nuclear magnetic resonance (NMR) spectra are shown in Figures S1 and S2 in Supporting Information. The polyethylene segments content of PEB is about 65% calculated from the ^{1}H NMR (Figure S2, Supporting Information). We confirmed the full conversion of the thiol-ene reaction via Fourier transform infrared (FTIR) spectroscopy, by monitoring the depletion of the characteristic S-H stretching vibration at 2563 cm^{-1} (Figure 1d). The obtained copolymer network (60 min curing) has a gel fraction of 40%, estimated by weighing the material before and after immersion in tetrahydrofuran (THF) for 24 h (Figure S3, Supporting Information).

We used small-angle X-ray scattering (SAXS), shown in Figure 1e and Figure S4 (Supporting Information), to monitor the crystallinity of the rubbery network. 2D SAXS patterns verify structural anisotropy induced by the stretching during cross-linking, from an initially isotropic network of randomly sized and distributed semi-crystalline domains. Such semi-crystalline domains result from the segregation of crystallites from amorphous PE segments. Note that external stress applied during the thiol-ene reaction determines both the alignment of the rubbery chains and the orientation of the PE crystallites. Stress-induced nanoscopic anisotropy consequently dictates the mode of macroscopic deformation of the rubber upon stimulation.

The crystalline domains of the PE also serve as physical connections in the rubbery networks (Figure 1a) that influence the thermomechanical properties of the rubber.[45] For instance, the non-uniform size of the PE segments results in a broad window of melting between 20 and 90 °C, as shown in Figure 1f by differential scanning calorimetry (DSC). Such a wide phase transition range enables tuning of thermal strain by adjusting the heat to be applied. Figure 1g shows the variation of the thermal strain against time at different temperatures for the semi-crystalline rubber sample, reaching a maximum of 28% at 90 °C followed by a plateau. Cyclic heat induced strain evolution, see Figure S5 (Supporting Information).

© 2022 The Authors. Advanced Functional Materials published by Wiley-VCH GmbH

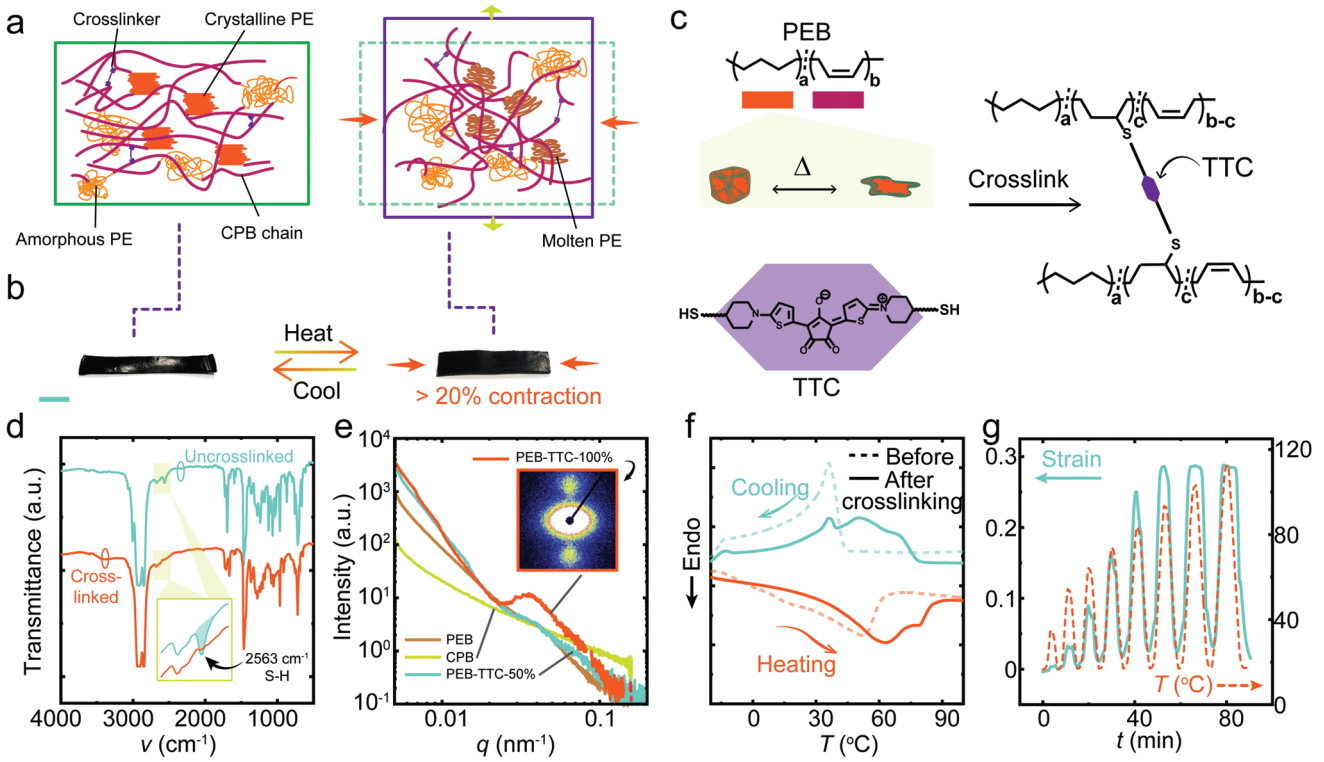

Figure 1. The material concept for the stimuli-responsive rubber. a) Schematic drawing of the deformation mechanism: melting/crystallization of the PE segments causes contraction/expansion of the rubbery network. b) Photographs of a sample deforming on a 90 °C hot plate. Scale bar: 5 mm. c) Chemical structure of the synthetic polyethylene-polybutadiene copolymer (PEB) and the reaction step of cross-linking to obtain PEB-TTC. d) FTIR spectra of PEB-TTC before and after UV curing. e) Small-angle X-ray scattering (SAXS) spectra of cis-1,4 polybutadiene (CPB), PEB, and PEB-TTC cross-linked under 50% (PEB-TTC-50%) and 100% (PEB-TTC-100%) stretching. Inset: the related SAXS pattern of PEB-TTC-100%. f) DSC curves of the uncured and cured PEB-TTC-100% during the first cooling and second heating cycle (10 °C min^{-1}). g) Evolution of deformation strain by varying the heating temperature. Sample size: $10 \times 2 \times 0.25$ mm^3, pre-elongation 100%.

2.2. Programmable Light-Driven Shape Changes

Prior to this work, a two-way shape-memory effect has been reported for PEB networks that have been physically cross-linked with hydrogen bonds.[46] Although such networks could be deformed, they suffered from creep and possessed only limited reversibility. Such issues are resolved in this work by the use of TTC for the covalent cross-linking of the PEB chains. TTC enables the fixation of permanently programmed geometries, yielding reversible thermoresponsive shape-morphing. Moreover, the high absorption of TTC results in a significant temperature elevation, up to > 180 °C, upon exposure to visible (532 nm, 633 nm) or NIR (808 nm) light (Figure S6, Supporting Information).

The shape-change programming can be achieved by UV-initiated thiol-ene cross-linking[47] during pre-straining the uncross-linked PEB to a desirable geometry. Both the percentage and geometry of the pre-strain, together with the cross-linking time, can be used to fine-tune the initial shape and the deformation profile. **Figure 2**a (top) shows uniaxially aligned PEB rubber, obtained by stretching and simultaneous UV exposure from both sides. Illuminating from both sides ensures uniform cross-linking and identical mechanical properties throughout the film thickness. The uniaxially aligned PEB-TTC actuator contracts upon photothermal heating and recovers its original shape after ceasing the irradiation (Figure 2a bottom).

In addition to the pre-straining profile, the duration of the UV-induced cross-linking can be utilized to control the initial shape and the extent of photothermal deformation. Figure 2b (top) shows a PEB rubber being cross-linked when exposed to UV from only one side while stretched. A light intensity gradient through the sample thickness during the cross-linking is created owing to the material absorption and scattering. Such gradient results in a higher cross-linking density (lower actuation strain) on the side closer to UV, which causes a bending toward the opposite direction. The schematic drawing of cross-linking densities upon UV irradiation is shown in the inset of Figure 2b. Figure 2b (bottom) shows the photothermal bending of the sample programmed via this technique. The effect of cross-linking time on the initial geometry and the photothermal bending under identical stimulation conditions is shown in Figure S7a (Supporting Information).

Also, the percentage of pre-strain during the cross-linking affects the achievable strain as it determines the extent of elongation of the rubbery chains during the cross-linking. Figure S7b (Supporting Information) shows the increase in bending angle for samples with higher pre-straining during cross-linking. We examined the extent of chain elongation by

© 2022 The Authors. Advanced Functional Materials published by Wiley-VCH GmbH

16163028, 2022, 41, Downloaded from https://onlinelibrary.wiley.com/doi/10.1002/adfm.202206939 by Tampere University Of Tech Tut, Wiley Online Library on [25/10/2022]. See the Terms and Conditions (https://onlinelibrary.wiley.com/terms-and-conditions) on Wiley Online Library for rules of use; OA articles are governed by the applicable Creative Commons License

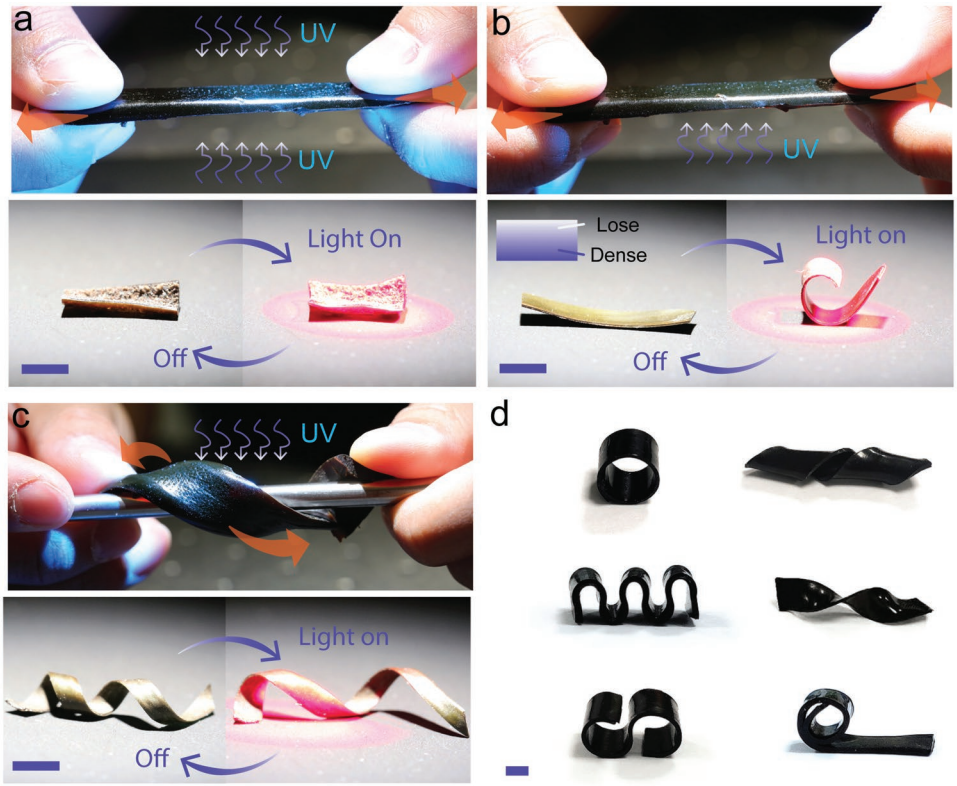

Figure 2. Shape programming of the rubber actuator. a) Schematics of cross-linking upon stretching under UV illumination from two sides (top), and photographs of uniaxial contraction upon light irradiation (bottom). b) Schematics of cross-linking upon stretching under UV illumination from one side (top) and photographs of the bending deformation upon light irradiation (bottom). c) Schematics of the UV curing upon an external force field (top), and photographs of the resulting actuator performing coiling and uncoiling controlled by light (bottom). d) Examples of different programmed shapes. In (a–c): Illumination condition, 633 nm, 800 mW cm^{-2}. Scale bars: 5 mm.

uniaxially stretching the rubbers during in situ wide-angle X-ray scattering (WAXS) analysis (Figure S8, Supporting Information). The orientational order parameter (S)[48] perpendicular to the stretching decreases from 0 to –0.13 for samples pre-strained from 0 to 200%, calculated by the Hermans formula (0 for randomly orientated polymer chains and –0.5 for a perfect alignment).[48] These results indicate that the higher the pre-strain of uncured samples, the higher the degree of alignment order within the polymer chains, which in turn enhances the photothermal actuation amplitude.

More complex geometries and shape-change profiles can be obtained using different pre-straining geometries during the cross-linking. Figure 2c (top) shows the shape-programming of the PEB rubber into a coil. The resulting construct exhibits a reversible change in the coil pitch under light irradiation (Figure 2c, bottom). Using the same strategy, we obtained various geometries and deformation profiles, some of that are shown in Figure 2d.

2.3. Load-Bearing and Resilience

Photothermal temperature increase beyond 100 °C causes the PE crystallites to melt, resulting in macroscopic contraction forces capable of lifting heavy objects. **Figure 3**a shows a strip of PEB-TTC rubber (uniaxially aligned, pre-elongated 100%, undergoing UV illumination from both sides) capable of reversibly lifting a load 3500 times its body weight (BW) (486 kPa) with an active strain of 27%. The load-bearing capability of the PEB-TTC rubber was tested at different light intensities, and the rubber maintained an active strain of >18% subject to loads of 10 000 times BW (1.4 MPa) with a work capacity of 220 J kg^{-1} (Figure 3b; Movie S1, Supporting Information). Regardless of the loading condition, the active strain for the tested actuators plateaued when the light intensity reached 700 mW cm^{-2}.

The large actuation strength is reflected by the material's modulus at >90 °C. As shown in Figure 3c, Young's modulus of the rubber decreases upon heating because of the melting of the crystalline PE segments (see Figure S9 in Supporting Information for more details on the mechanical testing). However, the modulus maintained a high value of ≈2.5 MPa at temperatures up to 140 °C. Muti-cycled stress versus strain diagram reveals good recovery and low hysteresis of the material upon passively induced deformation (inset of Figure 3c). Detailed mechanical measurements, i.e., testing the elastic limit and showing up to 50 stress–strain cycles at elevated temperatures, are shown in Figure S10 (Supporting Information). The large Young's modulus and resilience indicate good durability over cycles of load-bearing actuation.

Generally, bearing loads for multiple cycles may impose irreversible alterations to the polymer network, which adversely affects the active strain that highly depends on the specific

© 2022 The Authors. Advanced Functional Materials published by Wiley-VCH GmbH

16163028, 2022, 41, Downloaded from https://onlinelibrary.wiley.com/doi/10.1002/adfm.202206939 by Tampere University Of Tech Tut, Wiley Online Library on [25/10/2022]. See the Terms and Conditions (https://onlinelibrary.wiley.com/terms-and-conditions) on Wiley Online Library for rules of use; OA articles are governed by the applicable Creative Commons License

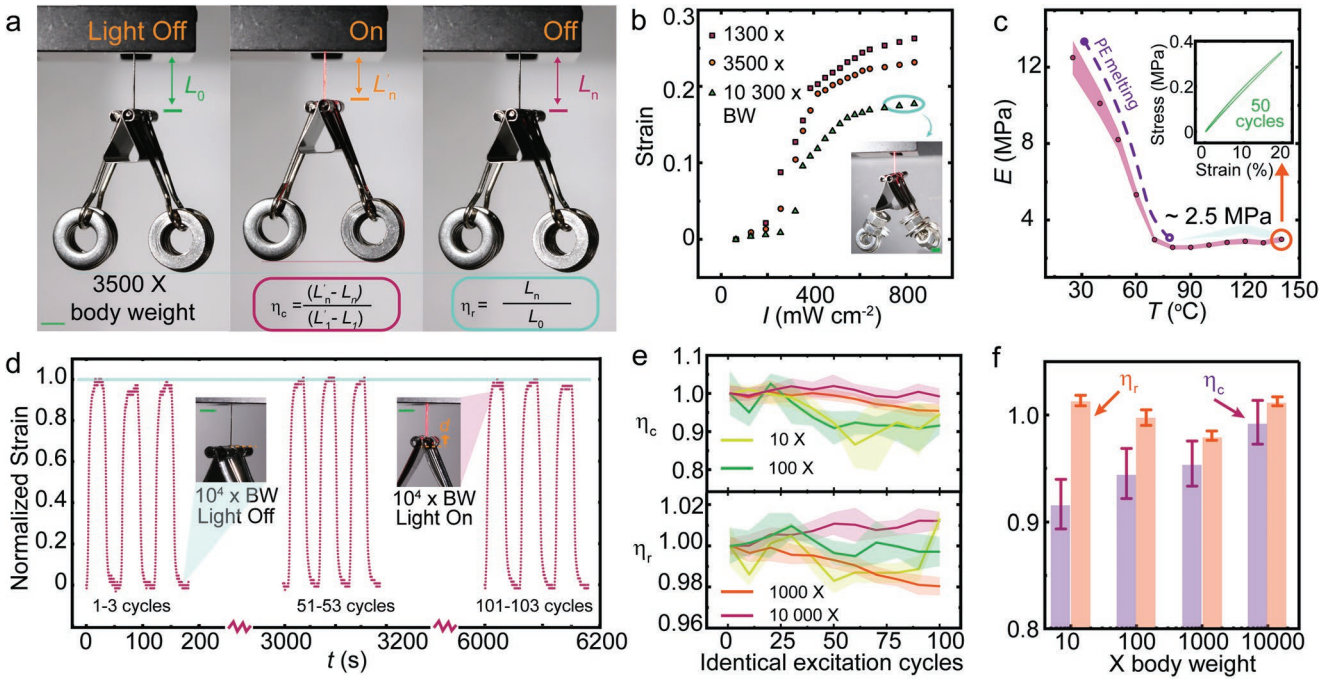

Figure 3. High-performance light actuation. a) Photographs of a photocontracting rubber lifting an object 3500× its BW (486 kPa). Light excitation: 633 nm, 500 mW cm^{-2}. b) Light-induced strain upon different loading. c) Young's modulus at different temperatures. Inset: 50 stress–strain cycles at 140 °C. d) Deformation strain during hundred light actuation cycles upon load of 10 000× BW (1.4 MPa). Insets: photographs of light-induced deformation. e) The deformation reversibility (η_c) and shape recovery (η_r) over 100 light actuation cycles and upon loads of 10×, 100×, 1000×, 10000× BW (1.4, 14, 140 kPa and 1.4 MPa). f) The reversibility after 100 light actuation cycles. Light excitation in (d–f): 633 nm, 710 mW cm^{-2}, 30 s light ON and 30 s light OFF. Error bars indicate standard deviation for $n = 3$ consequent measurements. All samples are pre-elongated 100%, and UV cured for 60 min from both sides (20 mW cm^{-2}). All scale bars: 5 mm.

amount of load. Figures S11 and S12 (Supporting Information) show the formulation and reversibility of strain for an exemplary LCE actuator. The soft LCE exhibits 4% shrinkage upon loading of 50 × BW (11 kPa) after one light actuation cycle. However, it is elongated by 3% after one heat-cool cycle upon loading of 1000 × BW (0.22 MPa). The irreversibility of material deformation depends on the amount of external loading, thus posing challenges for precise control of position/strain over multiple actuation cycles. Herein, to quantify the reversibility of the actuators' strain, we define two metrics: shape-recovery (η_r) and deformation reversibility (η_c) (see Figure 3a). Shape-recovery is defined as $\eta_r = L_n/L_0$, which shows the ratio between the length of the actuator at room temperature, or light off state (L_n), after n cycles of photothermal actuation and the length of the original actuator (L_0). The length measurements in both cases are carried out under a constant load. Deformation reversibility is defined as $\eta_c = (L'_n - L_n)/L'_1 - L_1)$, which shows the ratio between the deformation amplitude in the n^{th} cycle to that of the first cycle of actuation, under identical loading conditions. L'_n is the length of the photothermally deformed actuator (in the n^{th} cycle), or light on state, while L_n represents the length of the same actuator at room temperature or light off state.

Figure 3d,e shows the durability and reversibility of the PEB-TTC actuator under loads ranging from 10× to 10 000× BW (1.4 kPa–1.4 MPa), for over 100 actuation cycles under identical conditions (633 nm, 710 mW cm^{-2}, 30 s light ON and 30 s light OFF). As can be seen in Figure 3d, the actuator shows negligible drift in its active strain when loaded by 10 000× BW (1.4 MPa). The shape-recovery (η_r) after 100 actuation cycles remains as high as 99.7% upon the application of 100× BW (14 kPa) and shows up to 2% drift under 10 000× BW load (1.4 MPa). The deformation reversibility (η_c) shows a decrease after 20 cycles but maintains a plateau at ≈90% for all applied loads. While it appears that there is no direct correlation between η_r and the applied load, η_c seems to increase with the loading. Such increase may be attributed to the higher alignment order and chain orientation achieved under larger loads, which results in better reversibility.[20]

2.4. Robotic Applications

The reversible deformation and resilience of the light active rubber can be employed for a variety of light-fueled robotic functionalities, such as spatially controlled shape-morphing,[49,50] locomotion,[51,52] and heavy cargo transport.[24] For the photo-induced shape-morphing, precise localization of stimulating light can be used for the spatial control of deformation in an active rubbery construct, as shown by the selective movement of humanoid parts in **Figure 4**a. Figure 4b shows a long strip of rubber that undergoes a large coiling deformation upon illumination. For locomotive function, a light-driven walker is shown in Figure 4c and Movie S2 (Supporting Information). By switching the light on and off, the actuator cyclically deforms and moves in the desired direction, which is dictated by the

© 2022 The Authors. Advanced Functional Materials published by Wiley-VCH GmbH

16163028, 2022, 41, Downloaded from https://onlinelibrary.wiley.com/doi/10.1002/adfm.202206939 by Tampere University Of Tech Tut, Wiley Online Library on [25/10/2022]. See the Terms and Conditions (https://onlinelibrary.wiley.com/terms-and-conditions) on Wiley Online Library for rules of use; OA articles are governed by the applicable Creative Commons License

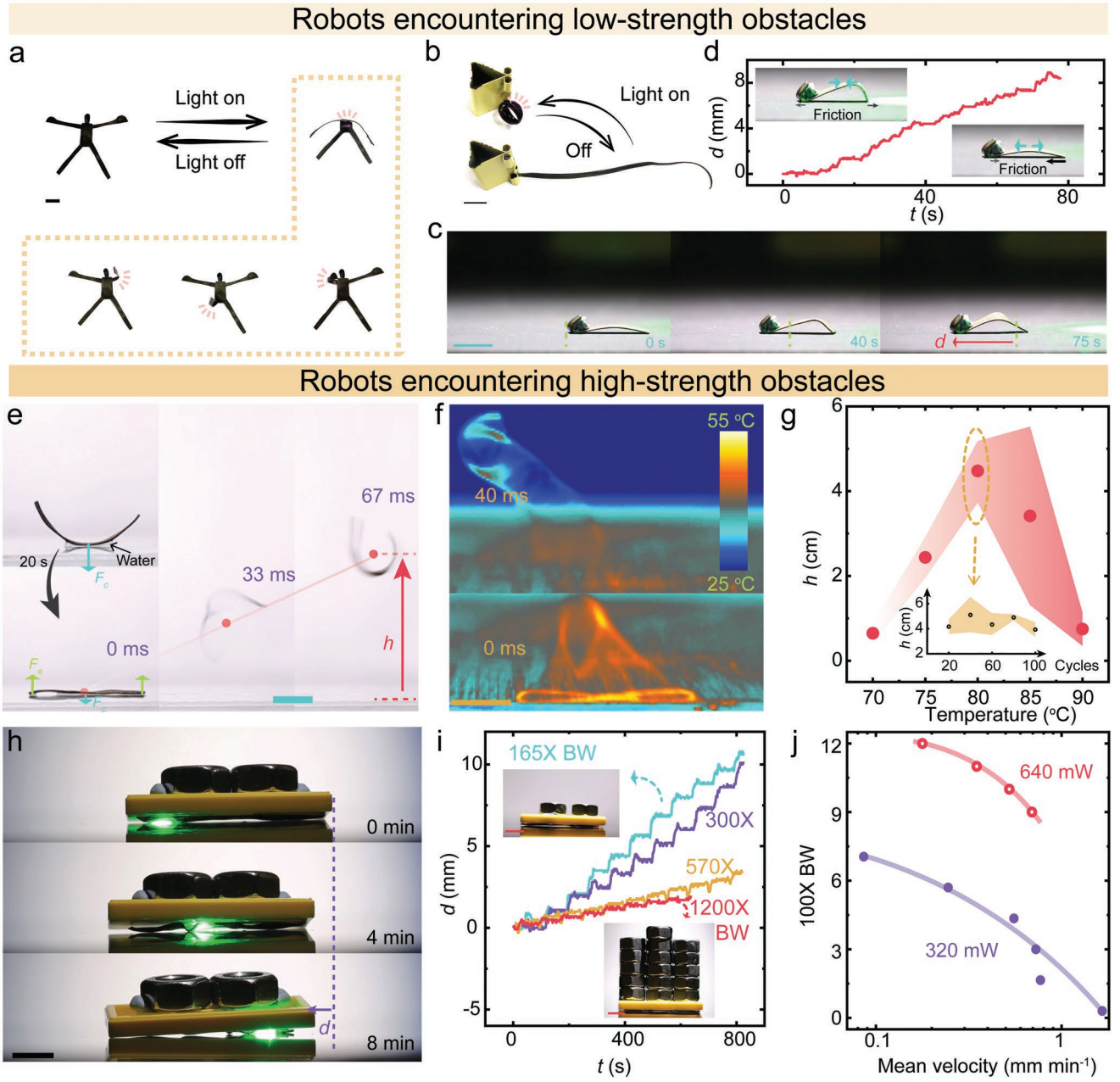

Figure 4. Soft robots based on the active rubber. a) Photographs of humanoid assembly exhibiting controlled movements upon light excitations (808 nm, 1 W cm^{-2}). b) A long bending strips showing tendril-like deformation upon light excitation (808 nm, 2.5 W cm^{-2}). c) An asymmetric walker performing inching movement upon temporally modulated light excitation (532 nm, 0.8 W cm^{-2}). d) The walking trajectory from (c). Insets: the strength of experienced friction upon illumination and after ceasing the light. e) Snapshots of a strip jumping on a capillary hot plate through releasing the stored elastic energy. Substrate temperature: 80 °C. The pre-bending of the structure is due to the release of internal stress inside the material. f) Thermal camera images of the jumping process. g) The jumping height of the rubbery strip at different temperatures. Error bars indicate standard deviation for $n = 3$ measurements. Actuator dimension: $22 \times 2 \times 0.2$ mm^3. h) Photograph of the rubber actuator carrying and translocating a 165× BW load upon scanning a laser beam. Laser: 532 nm, spot size 4 mm, power 320 mW. Scanning speed, 0.9 mm s^{-1}. Actuator dimension: $20 \times 3 \times 0.2$ mm^3. i) Light-fueled walking distance (d) under different loads. 320 mW laser excitation for 165, 300, 570× BW; 640 mW for 1200× BW. j) The walking mean velocity (v) under different loads. Scanning speed in (h–j): 0.9 mm s^{-1}. All scale bars are 5 mm. All samples are pre-strained by 100% and UV cured from one side (20 mW cm^{-2}, 60 min).

location, speed, and mode of illumination (Figure 4c,d). The key to achieving directional locomotion is the friction bias produced by asymmetric leg structures that undergo cyclic movements. When the strip bends to reduce the leg-distance (light ON), it experiences similar frictions from both sides; when the strip unbends to expand (light OFF), the friction on the back leg is significantly larger than the former, as schematically shown in the insets of Figure 4d. Cyclic deformation on

© 2022 The Authors. Advanced Functional Materials published by Wiley-VCH GmbH

16163028, 2022, 41, Downloaded from https://onlinelibrary.wiley.com/doi/10.1002/adfm.202206939 by Tampere University Of Tech Tut, Wiley Online Library on [25/10/2022]. See the Terms and Conditions (https://onlinelibrary.wiley.com/terms-and-conditions) on Wiley Online Library for rules of use; OA articles are governed by the applicable Creative Commons License

the substrate yields a net motion toward the forward direction. The materials shown in Figure 4c are experiencing minimal external forces (same order of magnitude as BW or less) such as friction. Unlike these examples, robotic materials when encountering the interfaces should be able to perform specific functions under dynamic friction and to bear opposing friction/drag forces across a large range of amplitudes. The conventional light-responsive soft materials typically fail under such conditions.

We demonstrate the outstanding performance of the active rubbers developed in this work to overcome external forces such as friction in the following two examples. Figure 4e and Figure S13 (Supporting Information) show the jumping locomotion of a rubber strip placed on top of a droplet of water poised on a hot plate. Upon heating, the bent rubber strip, which is fixed by a transient capillary layer, flattens and stores elastic energy. Evaporation of the water layer eventually leads to a burst release of the stored elastic energy, which is sufficient to eject the rubber. Figure 4f and Movie S3 (Supporting Information) visualize the jumping through a thermal camera and Figure 4e and Movie S4 (Supporting Information) show the trajectory of the jumping over time. The maximum jumping height is observed at 80 °C hot stage, as shown in Figure 4g. This may be ascribed to the competition between the elastic energy-storing process upon heating and reduction in capillary force through water evaporation. Low hot plate temperature results in a small elastic strain and energy for triggering jumping, while high temperature causes fast evaporation of water, yielding a sudden drop of the capillary adhesion before a large amount of elastic energy is stored. The material deformation is fully reversible, allowing jumping performance over a hundred cycles without a decrease in efficiency, as shown in the inset of Figure 4g. The size-dependent jumping behavior is also shown in Figure S14 (Supporting Information).

The large work capacity of the PEB-TTC rubber at elevated temperatures along with its reversibility in deformation can be used for the transport of heavy cargo. Figure 4h and Movie S5 (Supporting Information) show the locomotion of a PEB-TTC strip carrying cargos weighing 165× BW on a flat substrate. The rubber strip center is fixed to the load by adhesive tape (2×1 mm^{-2}). The locomotion is obtained by scanning a laser beam underneath the glass substrate along the rubber strip (from left to right) that leads to a traveling local deformation of the strip. The high active force during the deformation results in the lifting of the load and its transport by the strip (from right to left). The friction between the strip and the glass substrate and the intensity and speed of the scanning laser beam dictates the speed of the locomotion. The locomotion speed varies between 0.18 to 1.7 mm min^{-1} when the strip carries 1200× BW to 30× BW (Figure 4i; Movie S6, Supporting Information). The kinetics of the locomotion is elaborated in detail in Figure S15 (Supporting Information). The speed, as shown in Figure 4j, decreases by increasing the load or by decreasing the laser power. More details about the traveling distance versus time at different scanning power and speed, see in Figure S16 (Supporting Information).

The static friction coefficient between the rubber and the glass substrate is measured to be ≈1.2. This indicates that the opposing force on the rubbery transporter is in the same order of magnitude as the gravitational force of the applied load. The ratio between the carried load and the bodyweight of various transporters made from responsive materials is shown in Figure S17 (Supporting Information). A comparison of load-bearing capacities between transporters with similar body sizes made from LCEs, magnetic and dielectric elastomers, and carbonaceous bilayers confirms the remarkable load-bearing capacity of our rubbery actuator. However, it must be noted that our rubbery transporter has a lower speed compared to other transporters on the list, although the velocity, in principle, can be elevated by increasing the laser power.

3. Discussion

Semi-crystalline phase transition as a driving mechanism for two-way shape-memory deformation has been reported in the literature.[42,53–56] In this study, we focus on actuation reversibility, which is key to the precise positional control of the robotic motion over multiple cycles of operation. We have quantified the actuation reversibility of our rubber actuators by two distinct metrics of deformation reversibility and shape-recovery rate, by systematically exposing them to identical light under different loads across four orders of magnitude (10× to 10 000× of the actuator weight, or 1.4 kPa to 1.4 MPa). In these measurements, the rubber actuators exhibit remarkable reversibility metrics: > 90% deformation repeatability and > 98% shape-recovery rate.

One important issue to be noticed is that, the actuator itself follows the physical scaling law,[57] i.e., heat capacity that dictates the heating-and-cooling rate, scales with L^3 (L is the characteristic length of the sample), active force scales with L^2, resonance frequency scales with L^{-1}. Govern by this scaling effect, any motions generally considered to be slow in macroscopic samples, i.e., ≈1 Hz in mm-sized LCE,[58] can be accelerated to 1000 Hz for a microscopic structure by using the same chemical composition.[59] The BW multiple is also length scale dependent, thus some scalable quantity such as active stress is deemed more suitable for comparing material metrics.

Upon light excitation, the energy is fully absorbed close to the sample surface due to the high absorbance. The heat is then transferred to the other surface through thermal conduction. Due to the small thickness (typically 0.1–0.2 mm), the temperature difference between two surfaces is rather small (<3 at 120 °C), as indicated by the Finite Element simulation in Figure S18 (Supporting Information). In this case, light excitation can be considered as a uniform heating source across the sample thickness, in contrast to the light absorption gradient in photoswitch-containing polymers.[60] The resulting deformations (bending, contraction or coiling) are thus predominantly determined by the polymer chain orientation as programmed during fabrication (Figure 2), and not by the temperature gradient.

4. Conclusion

To conclude, we report a programmable, resilient, light/heat-responsive soft robotic material based on synthetic polyethylene-co-polybutadiene rubber. The copolymer can be manually

© 2022 The Authors. Advanced Functional Materials published by Wiley-VCH GmbH

16163028, 2022, 41, Downloaded from https://onlinelibrary.wiley.com/doi/10.1002/adfm.202206939 by Tampere University Of Tech Tut, Wiley Online Library on [25/10/2022]. See the Terms and Conditions (https://onlinelibrary.wiley.com/terms-and-conditions) on Wiley Online Library for rules of use; OA articles are governed by the applicable Creative Commons License

programmed to show various deformations, while the specific performance can be fine-tuned by changes in UV exposure time and/or applied pre-strain during the cross-linking process. The polybutadiene chains enable high material modulus of 2.5 MPa upon actuation at elevated temperatures up to 140 °C, while the synergy between re-crystallization of polyethylene segments and the rubbery network guarantees excellent reversibility for light-induced deformation (>90%) and shape-recovery (>98%), measured over 100 actuation cycles upon loads from 10× to 10 000× of the actuator weight (1.4 kPa – 1.4 MPa). Two resilient locomotors are demonstrated that present sufficient energy to function and overcome opposing forces from their environment. First, a bending rubbery strip attached to a hot plate via capillary force can store elastic energy and perform a high jump by overcoming the adhesion upon water evaporation. Second, a rubber-based transporter is used to show the load-carrying capability using scanning laser stimulation. The transporter is capable of carrying loads up to 1200× its bodyweight and translocating directionally on a substrate, exhibiting the ability to execute tasks under extremely hindered conditions. This study provides a novel material for stimuli-responsive soft robotics. A detailed analysis of the actuation reversibility and stimuli-driven control of the developed soft actuator may further promote the cross-talk between micro-roboticists and material scientists.

5. Experimental Section

Materials in Brief: Cis-1,4-Polybutadiene (CPB, cis-1,4 content: 96.8%, Mn: 239 kg mol^{-1}, Mw/Mn: 2.6) was purchased from Dushanzi Petrochemical Company, PetroChina. Cis-1,4 polyethylene-polybutadiene semicrystalline copolymer (PEB) was prepared through the hydrogenation reaction of CPB using the reagents of *p*-toluenesulfonyl hydrazide (TSH) and tri-*n*-propylamine (TPA). The synthesis process was according to the reported method.[61] The synthesis of the photothermal dye, 2,5-Bis[(6-thiolhexyl-4-carboxylate-piperidylamino) thiophenyl]-croconium (TTC), is given in the Supporting Information .

PEB-TTC Preparation: TTC (0.4 g) and 2,2-dimethoxy-2-phenylacetophenone (DMPA) photoinitiator (5 mg) were added into a stirred solution (PEB, 1.0 g in THF, 50 mL). The addition amount of TTC was fixed at 9% of the double bonds on PEB chains. The mixture solution was cast onto a glass substrate and left at room temperature for 24 h. After evaporation of the THF solvent, the resultant film was further dried in a vacuum oven at 40 °C for 48 h. The samples were then irradiated with the 365 nm UV light (20 mW cm^{-2}) for polymerization.

Material Characterization: ^{1}H NMR and ^{13}C NMR spectra were collected in deuterated chloroform ($CDCl_3$) in a Varian Unity spectrometer (400 MHz). Tetramethylsilane (TMS) was used as an interior reference. Fourier transform infrared spectroscopy (FTIR) was measured by Bruker Vertex 70 spectrometer. In situ small angle, X-ray scattering (SAXS) experiments were performed on a Xenocs Xeuss 2.0 instrument connected with a Cu X-ray source and a detector (Pilatus 300 K, DECTRIS). Differential scanning calorimetry (DSC) analysis was carried out on a Q20 DSC (TA instrument) under N_2 atmosphere. Mechanical testing was performed in a dynamic mechanical analysis (DMA, Q800, TA). The temperature of the specimen surface was monitored by the thermal imager (FLUKE Ti7) during the mechanical testing, while the thermal images of the jumper were captured by an infrared camera (FLIR T420BX). In situ wide-angle X-ray scattering (WAXS) measurements were executed on a custom-designed micro-focus X-ray beam in a Xeuss system equipped with a Pilatus 100 K detector. UV–vis absorption spectra were recorded on a CARY 500 UV–vis–NIR Varian spectrophotometer.

Laser Excitation and Optical Imaging: For reversibility characterization, a beam from a laser diode (633 nm, 1 W, Roithner) was collimated by a plano-convex lens (focal length 75 mm, Thorlabs) and a plano-convex cylindrical lens (focal length 150 mm, Thorlabs), yielding 710 mW cm^{-2} at the sample plane. The laser power stability was ±1% over the 1.5 h measurement period. For the light-fueled walker experiment, a continuous laser beam from a solid-state DPSS laser (532 nm, 2 W, Roithner) was guided by mirrors to illuminate the bottom of the rubber strip through a glass substrate. The laser spot position was controlled by a motorized mirror (KDC101, Thorlabs). The excitation power was measured at the sample position. Optical images and video were recorded using a camera (Canon 5D Mark III, 100 mm lens). The sample position was tracked by using motion analysis software, Kinovea.

Supporting Information

Supporting Information is available from the Wiley Online Library or from the author.

Acknowledgements

This work was supported by National Natural Science Foundation of China (no. U1862206), the Academy of Finland (Academy Postdoc no. 331015, Research Fellow, no. 340263, project no. 324353) H.S. acknowledges the support from the Natural Sciences and Engineering Council of Canada (NSERC). The authors thank Feng Wang from Qingdao University of Science & Technology for the help in experiment. The work was conducted as part of the Finnish Center of Excellence programme on Life-Inspired Materials LIBER (no. 346107) and in the framework of the Finnish Flagship programme on Photonics Research and Innovation, PREIN (no. 320165).

Conflict of Interest

The authors declare no conflict of interest.

Data Availability Statement

The data that support the findings of this study are available from the corresponding author upon reasonable request.

Keywords

copolymers, light driven, locomotion, photo-actuations, soft robots, synthetic rubber

Received: June 17, 2022
Revised: July 13, 2022
Published online: August 5, 2022

[1] L. Hines, K. Petersen, G. Z. Lum, M. Sitti, *Adv. Mater.* **2017**, *29*, 1603483.
[2] S. I. Rich, R. J. Wood, C. Majidi, *Nat. Electron.* **2018**, *1*, 102.
[3] S. Kim, C. Laschi, B. Trimmer, *Trends Biotechnol.* **2013**, *31*, 287.
[4] M. Li, A. Pal, A. Aghakhani, A. Pena-Francesch, M. Sitti, *Nat. Rev. Mater.* **2021**, *7*, 235.
[5] G.-Z. Yang, J. Bellingham, P. E. Dupont, P. Fischer, L. Floridi, R. Full, N. Jacobstein, V. Kumar, M. McNutt, R. Merrifield, B. J. Nelson,

© 2022 The Authors. Advanced Functional Materials published by Wiley-VCH GmbH

16163028, 2022, 41, Downloaded from https://onlinelibrary.wiley.com/doi/10.1002/adfm.202206939 by Tampere University Of Tech Tut, Wiley Online Library on [25/10/2022]. See the Terms and Conditions (https://onlinelibrary.wiley.com/terms-and-conditions) on Wiley Online Library for rules of use; OA articles are governed by the applicable Creative Commons License

B. Scassellati, M. Taddeo, R. Taylor, M. Veloso, Z. L. Wang, R. Wood, *Sci. Robot.* **2018**, *3*, eaar7650.
[6] J. M. McCracken, B. R. Donovan, T. J. White, *Adv. Mater.* **2020**, *32*, 1906564.
[7] Z. Wang, Z. Wang, Y. Zheng, Q. He, Y. Wang, S. Cai, *Sci. Adv.* **2020**, *6*, eabc0034.
[8] J. Kim, J. A. Hanna, M. Byun, C. D. Santangelo, R. C. Hayward, *Science* **2012**, *335*, 1201.
[9] Z. Fang, H. Song, Y. Zhang, B. Jin, J. Wu, Q. Zhao, T. Xie, *Matter* **2020**, *2*, 1187.
[10] A. Lendlein, O. E. C. Gould, *Nat. Rev. Mater.* **2019**, *4*, 116.
[11] T. Xie, *Nature* **2010**, *464*, 267.
[12] J. Jiang, L. Han, F. Ge, Y. Xiao, R. Cheng, X. Tong, Y. Zhao, *Angew. Chem., Int. Ed.* **2022**, *61*, e202116689.
[13] T. H. Ware, M. E. McConney, J. J. Wie, V. P. Tondiglia, T. J. White, *Science* **2015**, *347*, 982.
[14] Y. Zhao, C. Xuan, X. Qian, Y. Alsaid, M. Hua, L. Jin, X. He, *Sci. Robot.* **2019**, *4*, eaax7112.
[15] H. Kim, S. Sundaram, J.-H. Kang, N. Tanjeem, T. Emrick, R. C. Hayward, *Proc. Natl. Acad. Sci. U S A* **2021**, *118*, e2024581118.
[16] Y. Y. Xiao, Z. C. Jiang, Y. Zhao, *Adv. Intell. Syst.* **2020**, *2*, 2000148.
[17] H. Zeng, P. Wasylczyk, D. S. Wiersma, A. Priimagi, *Adv. Mater.* **2018**, *30*, 1703554.
[18] Z. S. Davidson, H. Shahsavan, A. Aghakhani, Y. Guo, L. Hines, Y. Xia, S. Yang, M. Sitti, *Sci. Adv.* **2019**, *5*, eaay0855.
[19] H. E. Fowler, P. Rothemund, C. Keplinger, T. J. White, *Adv. Mater.* **2021**, *33*, 2103806.
[20] Q. He, Z. Wang, Y. Wang, Z. Wang, C. Li, R. Annapooranan, J. Zeng, R. Chen, S. Cai, *Sci. Robot.* **2021**, *6*, eabi9704.
[21] T. J. White, D. J. Broer, *Nat. Mater.* **2015**, *14*, 1087.
[22] K. M. Herbert, H. E. Fowler, J. M. McCracken, K. R. Schlafmann, J. A. Koch, T. J. White, *Nat. Rev. Mater.* **2022**, *7*, 23.
[23] M. Pilz da Cunha, S. Ambergen, M. G. Debije, E. F. G. A. Homburg, J. M. J. den Toonder, A. P. H. J. Schenning, *Adv. Sci.* **2020**, *7*, 1902842.
[24] Y. Zhai, T. N. Ng, *Adv. Intell. Syst.* **2021**, 2100085.
[25] S. Palagi, A. G. Mark, S. Y. Reigh, K. Melde, T. Qiu, H. Zeng, C. Parmeggiani, D. Martella, A. Sanchez-Castillo, N. Kapernaum, F. Giesselmann, D. S. Wiersma, E. Lauga, P. Fischer, *Nat. Mater.* **2016**, *15*, 647.
[26] H. Shahsavan, A. Aghakhani, H. Zeng, Y. Guo, Z. S. Davidson, A. Priimagi, M. Sitti, *Proc. Natl. Acad. Sci. U S A* **2020**, *117*, 5125.
[27] C. Ahn, X. Liang, S. Cai, *Adv.Mater. Technol.* **2019**, *4*, 1900185.
[28] J. Jeon, J. C. Choi, H. Lee, W. Cho, K. Lee, J. G. Kim, J.-W. Lee, K.-I. Joo, M. Cho, H.-R. Kim, J. J. Wie, *Mater. Today* **2021**, *49*, 97.
[29] M. Pilz da Cunha, H. S. Kandail, J. M. J. den Toonder, A. P. H. J. Schenning, *Proc. Natl. Acad. Sci. U S A* **2020**, *117*, 17571.
[30] J. Naciri, A. Srinivasan, H. Jeon, N. Nikolov, P. Keller, B. R. Ratna, *Macromolecules* **2003**, *36*, 8499.
[31] F. Lupi, D. Martella, S. Nocentini, D. Antonioli, M. Laus, D. S. Wiersma, C. Parmeggiani, *ACS Appl. Polym. Mater.* **2021**, *3*, 1602.
[32] K. Kumar, A. P. H. J. Schenning, D. J. Broer, D. Liu, *Soft Matter* **2016**, *12*, 3196.
[33] H. Shahsavan, S. M. Salili, A. Jákli, B. Zhao, *Adv. Mater.* **2017**, *29*, 1604021.
[34] M. Ouchi, T. Terashima, M. Sawamoto, *Chem. Rev.* **2009**, *109*, 4963.
[35] M. Tang, R. Zhang, S. Li, J. Zeng, M. Luo, Y. X. Xu, G. Huang, *Angew. Chem., Int. Ed.* **2018**, *57*, 15836.
[36] X. Qin, J. Wang, Y. Zhang, Z. Wang, S. Li, S. Zhao, T. Tan, J. Liu, L. Zhang, K. Matyjaszewski, *Adv. Funct. Mater.* **2020**, *30*, 2003429.
[37] N. Ning, S. Li, H. Wu, H. Tian, P. Yao, G.-H. Hu, M. Tian, L. Zhang, *Prog. Polym. Sci.* **2018**, *79*, 61.
[38] A. Shrivastava, *Introduction to plastics engineering*, William Andrew, , **2018**.
[39] I. Kolesov, O. Dolynchuk, D. Jehnichen, U. Reuter, M. Stamm, H.-J. Radusch, *Macromolecules* **2015**, *48*, 4438.
[40] N. Zheng, Y. Xu, Q. Zhao, T. Xie, *Chem. Rev.* **2021**, *121*, 1716.
[41] I. Apsite, S. Salehi, L. Ionov, *Chem. Rev.* **2022**, *122*, 1349.
[42] F. Ge, X. Lu, J. Xiang, X. Tong, Y. Zhao, *Angew. Chem., Int. Ed.* **2017**, *56*, 6126.
[43] M. Behl, K. Kratz, J. Zotzmann, U. Nöchel, A. Lendlein, *Adv. Mater.* **2013**, *25*, 4466.
[44] L. Liu, M. H. Liu, L. L. Deng, B. P. Lin, H. Yang, *J. Am. Chem. Soc.* **2017**, *139*, 11333.
[45] X. Wang, S. Zhan, Z. Lu, J. Li, X. Yang, Y. Qiao, Y. Men, J. Sun, *Adv. Mater.* **2020**, *32*, 2005759.
[46] Q. Yang, W. Zheng, W. Zhao, C. Peng, J. Ren, Q. Yu, Y. Hu, X. Zhang, *Polym. Chem.* **2019**, *10*, 718.
[47] Z. Liu, C. Yu, C. Zhang, Z. Shi, J. Yin, *ACS Macro Lett.* **2019**, *8*, 233.
[48] Y. Wang, Z. Jiang, Z. Wu, Y. Men, *Macromolecules* **2013**, *46*, 518.
[49] C. Li, Y. Xue, M. Han, L. C. Palmer, J. A. Rogers, Y. Huang, S. I. Stupp, *Matter* **2021**, *4*, 1377.
[50] G. M. Spinks, *Adv. Mater.* **2020**, *32*, 1904093.
[51] A. H. Gelebart, D. J. Mulder, M. Varga, A. Konya, G. Vantomme, E. W. Meijer, R. L. B. Selinger, D. J. Broer, *Nature* **2017**, *546*, 632.
[52] Y. Hu, Q. Ji, M. Huang, L. Chang, C. Zhang, G. Wu, B. Zi, N. Bao, W. Chen, Y. Wu, *Angew. Chem., Int. Ed.* **2021**, *60*, 20511.
[53] Q. Yang, C. Peng, J. Ren, W. Zhao, W. Zheng, C. Zhang, Y. Hu, X. Zhang, *Adv. Opt. Mater.* **2019**, *7*, 1900784.
[54] F. Ge, Y. Zhao, *Chem. Sci.* **2017**, *8*, 6307.
[55] J. Zhou, S. A. Turner, S. M. Brosnan, Q. Li, J. M. Y. Carrillo, D. Nykypanchuk, O. Gang, V. S. Ashby, A. V. Dobrynin, S. S. Sheiko, *Macromolecules* **2014**, *47*, 1768.
[56] Y. Gao, W. Liu, S. Zhu, *Macromolecules* **2018**, *51*, 8956.
[57] E. Diller, M. Sitti, *Found. Trend. Robot.* **2013**, *2*, 143.
[58] H. Zeng, O. M. Wani, P. Wasylczyk, A. Priimagi, *Macromol. Rapid Commun.* **2018**, *39*, 1700224.
[59] S. Nocentini, D. Martella, C. Parmeggiani, S. Zanotto, D. S. Wiersma, *Adv. Opt. Mater.* **2018**, *6*, 1800167.
[60] X. Pang, L. Qin, B.o Xu, Q. Liu, Y. Yu, *Adv. Funct. Mater.* **2020**, *30*, 2002451.
[61] C. K. Santin, M. M. Jacobi, R. H. Schuster, M. Santoso, *J. Therm. Anal. Calorim.* **2010**, *101*, 273.

© 2022 The Authors. Advanced Functional Materials published by Wiley-VCH GmbH

16163028, 2022, 41, Downloaded from https://onlinelibrary.wiley.com/doi/10.1002/adfm.202206939 by Tampere University Of Tech Tut, Wiley Online Library on [25/10/2022]. See the Terms and Conditions (https://onlinelibrary.wiley.com/terms-and-conditions) on Wiley Online Library for rules of use; OA articles are governed by the applicable Creative Commons License